Ao Li
School for Engineering of Matter,
Transport and Energy,
Arizona State University,
7442 E Tillman Avenue,
SIM 140,
Mesa, AZ 85212
e-mail: aoli5@asu.edu

Yan Chen[1]
The Polytechnic School,
Arizona State University,
7171 E Sonoran Arroyo Mall,
PRLTA 330M,
Mesa, AZ 85212
e-mail: yanchen@asu.edu

Xinyu Du
General Motors Global R&D,
Warren, MI 48090
e-mail: xinyu.du@gm.com

Wen-Chiao Lin
General Motors Global R&D,
Warren, MI 48090
e-mail: wen-chiao.lin@gm.com

Should a Vehicle Always Deviate to the Tire Blowout Side?—A New Tire Blowout Model With Toe Angle Effects

As a severe tire failure, tire blowout during driving can significantly threaten vehicle stability and road safety. Tire blowout models were developed in the literature to conclude that a vehicle always deviates to the tire blowout side. However, this conclusion is proved to be inaccurate in this paper, since one important factor was largely ignored in the existing tire blowout models. Toe angle, as a basic and widely applied setup on ground vehicles, can provide preset and symmetric lateral tire forces for normal driving. However, when tire blowout occurs, different toe angle setups can impact vehicle motions in different ways. For the first time, the toe angle is explicitly considered and integrated into a tire blowout model in this paper. For different tire blowout locations, driving maneuvers, and drivetrain configurations, the impacts of different toe angle setups on the variations of tire friction forces and vehicle motions are analyzed. The developed tire blowout model with toe angles is validated through both high-fidelity CARSIM simulation results and experimental results of a scaled test vehicle. Both simulation and experimental results show that a vehicle may not deviate to the tire blowout side, depending on the toe angle setups and driving maneuvers. Moreover, the experimental results also validate that the proposed tire blowout model can accurately evaluate the tire blowout impacts on vehicle dynamics. [DOI: 10.1115/1.4051034]

1 Introduction

Tires, as the only vehicle components directly interacting with the road, affect the dynamics and performance of a ground vehicle by providing nonlinear and coupled longitudinal and lateral friction forces. Healthy tires can provide desired vehicle handling performance, economical fuel consumption, and good riding comfort [1,2]. However, as a consumable item usually operating in an open environment, tire failures often occur. One specific and severe failure is the tire blowout, which often happens suddenly and cannot be completely avoided [3,4]. Various reasons can cause tire blowout, such as improper use (e.g., underinflating, overinflating, overloading), manufacturing defects, road hazards [5], inadequate tread depth, extreme climatic conditions (overheating) [6], and impact damages [7].

When tire blowout happens, vehicle stability can be suddenly violated by an additional yaw moment on the vehicle, which is caused by significant changes of tire friction forces between the normal tires and the blown-out tire(s). Consequently, the vehicle could rapidly deviate from the driving lane and collide with guardrails or other vehicles without appropriate control. Even worse, improper reactions from panic drivers, e.g., excessive steering and/or massive braking, can cause tire-rim separations and make the vehicle at the risk of rollover [6,8]. In 2015, the National Highway Traffic Safety Administration estimated that tire blowouts can cause more than 400 deaths and over 78,000 crashes every year [9]. Therefore, a sophisticated model is crucial and necessary to investigate tire blowout impacts on vehicle dynamics, which is the preliminary step toward vehicle stability control design for a tire blowout.

Over the past decades, many research works have been conducted on the modeling of tire blowout [6,10–18]. The general method to develop a tire blowout model is summarized in two steps. First, variations of some key tire parameters due to tire blowout are analyzed. Then, the parameter changes are integrated into a normal tire model to represent the varied tire forces due to tire blowout. Since many tire parameters are strongly coupled and affected by tire blowout simultaneously, different selections and considerations on the tire parameters were discussed in the literature. For example, two key tire parameters, lateral stiffness, and rolling resistance were simply considered in a tire blowout model with step changes [6,15]. Tire deflection time, tire radius, tire vertical force, lateral stiffness, and rolling resistance were discussed for a tire burst model [10,11]. The linear changes of lateral stiffness, camber stiffness, radial stiffness, tire effective radius, and rolling resistance were selected to develop a tire blowout model for simulation purposes [13,14,16]. With fewer impacts on vehicle dynamics compared with other parameters, the camber stiffness was typically neglected [17]. In sum, one common conclusion, which is that the vehicle would deviate to the tire blowout side, was drawn based on simulation results of many existing tire blowout models in the literature [10–14].

Although many different parameters and their variations were discussed, one key parameter, namely, toe angle, was not discussed and explicitly integrated into a tire blowout model in the literature. As shown in Fig. 1, the steering angles of the left and right tires are antisymmetric with respect to the vehicle longitudinal axis. In contrast, left and right toe angles are symmetric with respect to the vehicle longitudinal axis [19]. With the symmetric feature, the small toe angle on production vehicles can be set by adjusting the distance between the leading (or tail) edges of a pair of tires on the same axle. Specifically, the toe-in indicates the two leading edges are closer to each other, while the toe-out implies the two tail edges are closer to each other [20].

In the modeling of a tire blowout, the toe angle is necessary and important to be included for two main reasons. First, toe angle setups are widely applied in production vehicles for vehicle handling performance and suspension design. To enhance the straight-line driving stability, front wheel drive (FWD) vehicles usually have a

[1]Corresponding author.

Contributed by the Dynamic Systems Division of ASME for publication in the JOURNAL OF DYNAMIC SYSTEMS, MEASUREMENT, AND CONTROL. Manuscript received November 2, 2020; final manuscript received April 19, 2021; published online June 17, 2021. Assoc. Editor: Mahdi Shahbahkti.

front toe-out setup, since the longitudinal forces of front tires will rotate the wheels to align with the central line during driving. On the contrary, the front toe-in setup is usually applied for rear wheel drive (RWD) vehicles, where the rolling resistance forces of front tires are utilized for centralization [20]. Moreover, the aforementioned toe angle setups are not unique. For example, to improve vehicle cornering behaviors, front toe-out can be applied to RWD vehicles although the straight driving performance may be sacrificed [21]. In addition to influences on vehicle handling performance, toe angle setups are also used to balance camber forces for alleviating tire wear, when camber angles exist. Correspondingly, toe-in (toe-out) is required for a positive (negative) camber [22]. Based on the aforementioned discussions, different toe angle setups are widely designed and applied for different purposes.

Second, toe angles can be modeled as special and preset steering angles, with a symmetric and balanced feature on the left and right vehicle sides. Correspondingly, preset lateral friction forces exist, with the same magnitudes in an opposite direction, when symmetric toe angles are applied. In a normal straightforward driving scenario without tire blowout, the preset lateral friction forces due to toe angles can balance each other and will not influence vehicle motions. However, in the case of a tire blowout, the preset lateral forces introduced by toe angles and their (force and thus moment) variations before and after a tire blowout will significantly impact vehicle dynamics. Moreover, different toe angle setups can have diverse impacts on vehicle dynamics after a tire blowout.

It is worth noting that camber angle, caster angle, and kingpin inclination angle are also widely applied in production vehicles for wheel alignment. However, with fewer impacts on vehicle dynamics in the tire blowout situation, which are verified and discussed through simulation results in this paper, these wheel alignment parameters are neglected in the tire blowout model.

In this paper, four main contributions are summarized. First, the toe angle is explicitly formulated in a tire blowout model to describe its influences. Second, through MATLAB/SIMULINK and CARSIM cosimulation, the impacts of different toe angle setups on vehicle dynamics before and after a tire blowout are explored and analyzed for different tire blowout locations, driving maneuvers, and drivetrain configurations. Third, different tire blowout experiments are conducted on a scaled test vehicle for the validation of the proposed tire blowout model and analyses. Consistent observations from repeated simulation and experiment results reveal the toe angle influence on vehicle dynamics after tire blowout. The fact that a vehicle may not deviate to the tire blowout side is discovered, which will depend on vehicle driving maneuvers and toe angle setups. Last, the accuracy of the proposed tire blowout model to describe tire blowout influence on vehicle dynamics is also experimentally validated.

The rest of this paper is organized as follows. In Sec. 2, a new tire blowout model is developed by explicitly formulating toe angle setups. Simulation results and analyses of toe angle influences after tire blowout are presented in Sec. 3. In Sec. 4, the toe angle effects on tire blowout and model accuracy are validated through experiments on a scaled test vehicle. The conclusions are described in Sec. 5.

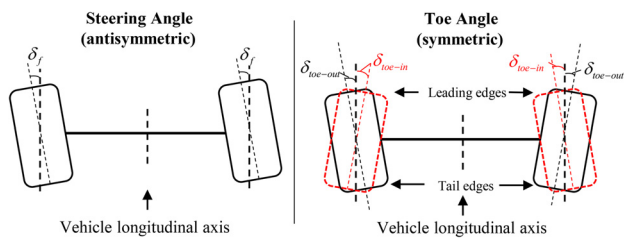

Fig. 1 Schematic of the steering angle and toe angle setups

2 Tire Blowout Modeling

In this section, a new tire blowout model is developed in three steps to explicitly incorporate toe angle setups. First, the changes of the selected key parameters about tire blowout are discussed in Sec. 2.1. Second, the tire force model integrated with the changed tire parameters and toe angles is introduced in Sec. 2.2. Third, to apply the developed tire blowout model, a vehicle dynamic model, and the simulation framework with the vehicle mathematical model and the vehicle CARSIM model are described and discussed in Secs. 2.3 and 2.4, respectively.

2.1 Changes of Tire and Vehicle Parameters Due to Tire Blowout. With the rapid and explosive process of a tire blowout, the tire tread, sidewall, and even structure will have abrupt deformation. Correspondingly, the tire longitudinal stiffness C_x, lateral stiffness C_y, radial stiffness C_r, and tire effective radius R_e will decrease rapidly. Since the tire-ground contact patch will be enlarged due to tire deflation, the rolling resistance coefficient K_r will increase.

In this work, a linear variation over the tire blowout duration Δt is adopted to model the changed key tire parameters before and after a tire blowout [13,18], as shown in Fig. 2. The reduction of the tire radial stiffness C_r is indirectly modeled and reflected in the changes of the contact patch length, tire effective radius R_e, vehicle pitch/roll disturbance, and the tire vertical force redistribution. Note that Fig. 2 only represents the linear variation trend of key tire parameters and the exact values are shown in the simulation section.

2.2 Tire Force Modeling. To investigate tire force changes before and after a tire blowout with the linearly varied tire parameters in Sec. 2.1, the well-known Dugoff's tire model [23] is utilized to calculate the nonlinear and coupled longitudinal and lateral friction forces, F_x and F_y, as described in the following equations:

$$F_x = f_x(C_x, C_y, F_z, s, \alpha, \mu) \tag{1}$$

$$F_y = f_y(C_x, C_y, F_z, s, \alpha, \mu) \tag{2}$$

where the longitudinal slip ratio and tire slip angle are denoted as s and α, respectively. F_z is the vertical force of the tire. μ is the tire-road friction coefficient.

For simplicity, indexes, $i = 1, 2, 3, 4$, denote the subscripts for the front left, front right, rear left, and rear right tires, respectively. The wheel dynamics are calculated in the following equation:

$$I_{\omega i}\dot{\omega}_i = T_i - R_{ei}(F_{xi} - F_{ri}) \tag{3}$$

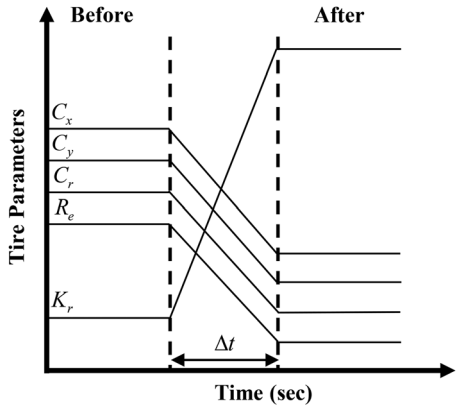

Fig. 2 Linear variations of key tire parameters before and after a tire blowout

where $I_{\omega i}$, ω_i, T_i, and R_{ei} represent the moment of inertia, wheel rotational speed, actuation torque, the effective radius of each tire, respectively. F_{xi} and F_{ri} are the longitudinal force and rolling resistance force on each tire, respectively. The wheel dynamics (3) is not only utilized to calculate the wheel rotational speed of the normal tires but also for the blown-out tire to obtain the wheel speed change, by applying the linearly varied tire effective radius R_{ei} of the blown-out tire.

The tire slip ratio s_i for each tire is defined in the following equation:

$$s_i = \frac{R_{ei}\omega_i - v_x}{\max(R_{ei}\omega_i, v_x)} \tag{4}$$

where v_x is the vehicle longitudinal velocity. Similarly, the tire slip ratio of the blown-out tire can be obtained with the linearly varied tire effective radius R_{ei}.

Next, the toe angle setup is considered and integrated into the tire slip angle calculation for the tire blowout modeling. For a typical vehicle with a front wheel steering, the front steering angles are assumed to be the same and rear steering angles are zero, $\delta_1 = \delta_2 = \delta_f$ and $\delta_3 = \delta_4 = 0$. When a toe angle setup is considered, the actual steering angle for each front tire is a combination of the steering angle and the front toe angle, and the actual steering angle for each rear tire is purely determined by the rear toe angle, as defined in the following equation [24]:

$$\begin{cases} \delta_1 = \delta_f - \delta_{\text{toef}} \\ \delta_2 = \delta_f + \delta_{\text{toef}} \\ \delta_3 = -\delta_{\text{toer}} \\ \delta_4 = \delta_{\text{toer}} \end{cases} \tag{5}$$

where δ_{toef} and δ_{toer} $\left(\delta_{\text{toej}}, j = f, r\right)$ represent the front and rear toe angle, respectively. Since the positive direction of the angle is counterclockwise, a positive δ_{toej} represents a toe-in setup, while a negative δ_{toej} represents a toe-out setup in Eq. (5). Without loss of generality, the geometric relationship in Eq. (5) about the front toe-in setup is presented in Fig. 3 as an example. The toe-out case and toe angle setups on rear tires can be described accordingly.

Therefore, the slip angle α_i for each tire with respect to the actual steering angle is depicted in the following equation:

$$\alpha_i = \begin{cases} \arctan\left(\dfrac{v_y + l_f r}{v_x}\right) - \delta_i, \ i = 1, 2 \\ \arctan\left(\dfrac{v_y - l_r r}{v_x}\right) - \delta_i, \ i = 3, 4 \end{cases}, \tag{6}$$

where l_f and l_r are the distance from the front axle to the vehicle center of gravity (CG) and the distance from the rear axle to the CG, respectively. r is the yaw rate and v_y denotes the lateral velocity.

The tire vertical forces F_{zi} in the Dugoff's tire model can be utilized to incorporate the variation of tire radial stiffness, suspension rearrangement, and pitch/roll disturbance. The tire vertical forces for normal driving without tire blowout are defined in the following equation [25]:

$$\begin{cases} F_{z10} = \dfrac{m}{2(l_f + l_r)}(l_r g - a_x h_g) - \dfrac{m}{(l_f + l_r)}(l_r g - a_x h_g)\dfrac{h_g}{l_t g} a_y \\ F_{z20} = \dfrac{m}{2(l_f + l_r)}(l_r g - a_x h_g) + \dfrac{m}{(l_f + l_r)}(l_r g - a_x h_g)\dfrac{h_g}{l_t g} a_y \\ F_{z30} = \dfrac{m}{2(l_f + l_r)}(l_f g + a_x h_g) - \dfrac{m}{(l_f + l_r)}(l_f g + a_x h_g)\dfrac{h_g}{l_t g} a_y \\ F_{z40} = \dfrac{m}{2(l_f + l_r)}(l_f g + a_x h_g) + \dfrac{m}{(l_f + l_r)}(l_f g + a_x h_g)\dfrac{h_g}{l_t g} a_y \end{cases} \tag{7}$$

where h_g is the height of CG and l_t is the wheel track. a_x and a_y are the longitudinal and lateral accelerations, respectively. m is the vehicle mass.

When one tire blows out, an additional load transfer Δf due to tire blowout will be generated. With the reduction of tire radial stiffness, suspension rearrangement, and pitch/roll disturbance, the suspensions at the blown-out tire and the corresponding diagonal one are stretched, while the other two suspensions are compressed. Consequently, the vertical forces of the blown-out tire and the diagonal one decrease, while the other two increase, with the same magnitudes [10,11]. Assuming that the front left $(i = 1)$ or rear right $(i = 4)$ tire is the blown-out tire without loss of generality, the above changes of tire vertical forces are determined in the following equation:

$$\begin{cases} F_{z1} = F_{z10} - \Delta f \\ F_{z2} = F_{z20} + \Delta f \\ F_{z3} = F_{z30} + \Delta f \\ F_{z4} = F_{z40} - \Delta f \end{cases} \tag{8}$$

To obtain the Δf in Eq. (8), the geometric relationship between the suspension height h_{si} and the tire effective radius R_{ei} is utilized, as shown in the following equation [26]:

$$R_{e1} + R_{e4} + h_{s1} + h_{s4} = R_{e2} + R_{e3} + h_{s2} + h_{s3} \tag{9}$$

The initial suspension heights are denoted as h_{s0i} and all initial suspension heights are equal. The relationships between the vertical forces and the suspension heights are given in the following equation:

$$h_{si} = h_{s0i} - \frac{F_{zi}}{K_{sk}}, \ (i = 1, 2, 3, 4) \tag{10}$$

where $K_{sk}(k = f, r)$ represents the front and rear suspension vertical stiffness, respectively. Therefore, the load transfer Δf due to tire blowout can be obtained based on Eqs. (8)–(10), as given in the following equation:

$$\Delta f = \frac{K_{sf}K_{sr}\Delta R - K_{sr}(F_{z20} - F_{z10}) - K_{sf}(F_{z30} - F_{z40})}{2(K_{sf} + K_{sr})} \tag{11}$$

where $\Delta R = R_e - R_t$. R_t is the effective radius changing linearly from the original value to the final value over the tire blowout duration Δt. Therefore, ΔR varies linearly.

The rolling resistance force F_{ri} is described as

$$F_{ri} = K_r F_{zi} \tag{12}$$

where K_r is the rolling resistance coefficient.

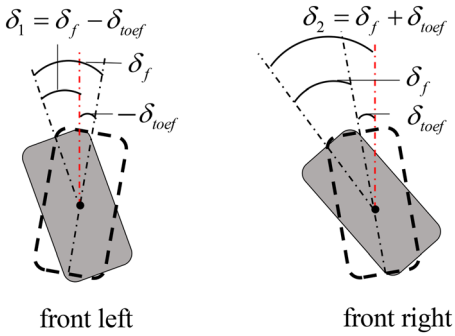

Fig. 3 Geometric relationship about front toe-in setup

2.3 Vehicle Dynamic Model. To explore the impacts of tire blowout on vehicle motions, the tire force variations due to tire blowout, as modeled in Sec. 2.2, need to be applied to a vehicle dynamic model. The vehicle dynamic model is shown in Eq. (13), based on Fig. 4.

$$\begin{cases} m(\dot{v}_x - v_y r) = \sum_{i=1}^{4}\left[(F_{xi} - F_{ri})\cos\delta_i - F_{yi}\sin\delta_i\right] \\ m(\dot{v}_y + v_x r) = \sum_{i=1}^{4}\left[F_{yi}\cos\delta_i + (F_{xi} - F_{ri})\sin\delta_i\right] \\ I_z\dot{r} = M_{zx} + M_{zy} \end{cases} \tag{13}$$

where I_z is the moment inertia through CG. $M_{zx} + M_{zy}$ is the total yaw moment applied to the CG, which is calculated using the longitudinal friction force, lateral friction force, and the roll resistance force of each tire. With certain steering angle and toe angle, the aforementioned tire forces can be decomposed in the local x–y coordinate. The moment portion from the tire forces in the x-direction and that from the tire forces in the y-direction are denoted as M_{zx} and M_{zy}, respectively, which are given in the following equation:

$$\begin{cases} M_{zx} = \dfrac{l_t}{2}\begin{bmatrix}(F_{x2} - F_{r2})\cos\delta_2 - F_{y2}\sin\delta_2 \\ +(F_{x4} - F_{r4})\cos\delta_4 - F_{y4}\sin\delta_4\end{bmatrix} \\ \quad -\dfrac{l_t}{2}\begin{bmatrix}(F_{x1} - F_{r1})\cos\delta_1 - F_{y1}\sin\delta_1 \\ +(F_{x3} - F_{r3})\cos\delta_3 - F_{y3}\sin\delta_3\end{bmatrix} \\ M_{zy} = l_f\sum_{i=1}^{2}\left[F_{yi}\cos\delta_i + (F_{xi} - F_{ri})\sin\delta_i\right] \\ \quad -l_r\sum_{i=3}^{4}\left[F_{yi}\cos\delta_i + (F_{xi} - F_{ri})\sin\delta_i\right] \end{cases} \tag{14}$$

Note that the positive directions of the local x–y coordinate and the global X–Y coordinate are also defined in Fig. 4. In the local x–y coordinate, the positive direction of F_x, F_r, and v_x is in the forward. Moreover, the positive direction of F_y and v_y is toward the left. M_{zx}, M_{zy}, and r have a counterclockwise positive direction. In the global X–Y coordinate, the left deviation (lateral offset) is positive, while the right deviation is negative. The positive directions will be utilized in the analysis of simulation and experimental results.

Remark 1. Integrating the proposed tire blowout model with the vehicle model (13), the tire blowout effects with different toe angles on vehicle motions can be investigated. Moreover, the vehicle mathematical model (13) can also be replaced by a high-fidelity CARSIM model, in which different drivetrains, suspensions, and other wheel parameters (caster, camber, and kingpin inclination angles) can also be explored, in addition to the toe angle setup. In the simulation section, the simulation results with the vehicle mathematical model (13) and with the CARSIM model are compared to verify the significance of toe angle setups over other wheel parameters for the tire blowout modeling.

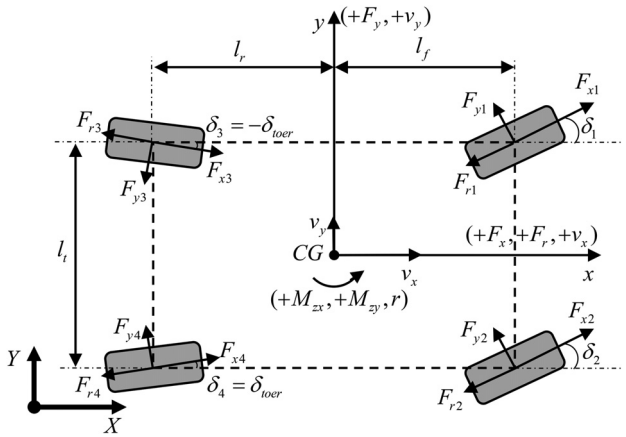

Fig. 4 Vehicle dynamic model with a rear toe-in setup

2.4 The Framework of Tire Blowout Model. Integrating the (sub)models in Secs. 2.1–2.3, the simulation framework of the proposed tire blowout model is shown in Fig. 5. The proposed tire blowout model (in the dashed box) is defined in MATLAB/SIMULINK. By applying predefined toe angle setups (5) to the slip angle calculation (6), together with the varied friction forces in Eqs. (1), (2), and (12) using changed tire parameters to the mathematical model (13), the tire blowout impacts including toe angle setups on vehicle dynamics can be investigated. When a CARSIM vehicle model is utilized, the longitudinal and lateral forces should be replaced by the varied friction forces. Moreover, the additional load transfer (11) needs to be added.

3 Simulation Results and Analyses

Using the proposed tire blowout model in Sec. 2, the impacts of different toe angle setups on vehicle dynamics after tire blowout are investigated comprehensively through different simulations and detailed analyses.

3.1 Comparison of Toe Angle Impacts With Other Wheel Alignment Parameters. In this section, the impacts of toe angles after tire blowout are compared with other wheel alignment parameters (caster, camber, and kingpin inclination angles) using the mathematical model (13) and a CARSIM vehicle model. The parameters of the adopted CARSIM C-Class hatchback vehicle are shown in Table 1. The final values of parameters are utilized to characterize the tire properties after tire blowout. The tire blowout duration is set as 0.3 s, which is achieved by a similar valve-based tire blowout device for the experiment, like that in Ref. [10]. At the fifth second of the total 10 s simulation time, the tire blowout is triggered. The absolute value of toe angle is set at 0.5 deg for both toe-in and toe-out setups, which is a reasonable setup considering that toe angle setup on production vehicles is typically less than 1 deg [19].

For comparison, the parameters of the CARSIM C-Class vehicle are also applied in the mathematical model (13). The same proportional–integral–derivative speed controller, providing driving torques to wheel dynamics in Eq. (3), is adopted for both mathematical and CARSIM models, to exclude the drivetrain difference in the two models. Therefore, with the suspension and kingpin structures, simulations using the CARSIM model can reflect the lumped impacts of toe angle and other wheel alignment parameters, while the mathematical model can only demonstrate the impacts of toe angles. Two simulation cases are studied as follows.

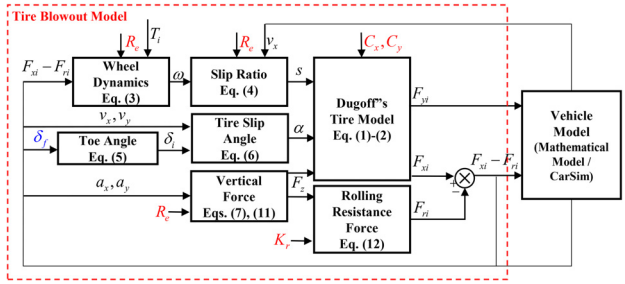

Fig. 5 Simulation framework of the tire blowout model

Table 1 Parameters of the C-class hatchback vehicle

Parameter	Symbol	Value	Final value
Vehicle parameters			
Vehicle total mass	m	1412 kg	—
Moment inertia around CG	I_z	1536.7 kg/m^2	—
Distance from front axle to CG	l_f	1.105 m	—
Distance from front axle to CG	l_r	1.895 m	—
Wheel track	l_t	1.675 m	—
Height of CG	h_g	0.54 m	—
Front suspension stiffness	K_{sf}	27,000 N/m	—
Rear suspension stiffness	K_{sr}	30,000 N/m	—
Tire parameters			
Tire effective radius	R_e	0.325 m	To 2/3
Longitudinal stiffness	C_x	47,000 N/slip	To 1/10
Lateral stiffness	C_y	−55,000 N/rad	To 1/10
Wheel moment inertia	I_w	0.9 kg/m^2	—
Rolling resistance coefficient	K_r	0.018	To 30 times

In the first case, different toe angle setups are applied with the same other wheel alignment parameters in the CARSIM vehicle model. The vehicle is driven in a straight line at a constant driving speed of 100 km/h (62 mph). Front left $(i = 1)$ and rear right $(i = 4)$ tire blowout are considered.

The simulation results for lateral offsets are compared in Fig. 6. For simplicity, the legend (0, 0) stands for the zero toe setups of (front, rear) tires. (in, 0) stands for (front toe-in, rear zero toe) and other toe angle setups can be represented accordingly. If the tire blowout does not happen, the vehicle is driven straightly and the lateral offset is always zero. In Figs. 6(*a*) and 6(*b*) about front left $(i = 1)$ and rear right $(i = 4)$ tire blowout, for each toe angle setup, other fixed wheel alignment parameters have small impacts on vehicle dynamics after a tire blowout, since the model difference (in the percentage of the offset difference at the end) are small as labeled in the zoom-in plots. Moreover, vehicle motions, in terms of the magnitude of lateral offset and deviation direction, are strongly affected by different toe angle setups, given that other fixed wheel alignment parameters are considered in the CARSIM model.

In the second case, the toe angle is fixed (0.5 deg, (in, 0)) for both models. One of other three wheel alignment parameters will change to solely explore its effects on tire blowout. The original

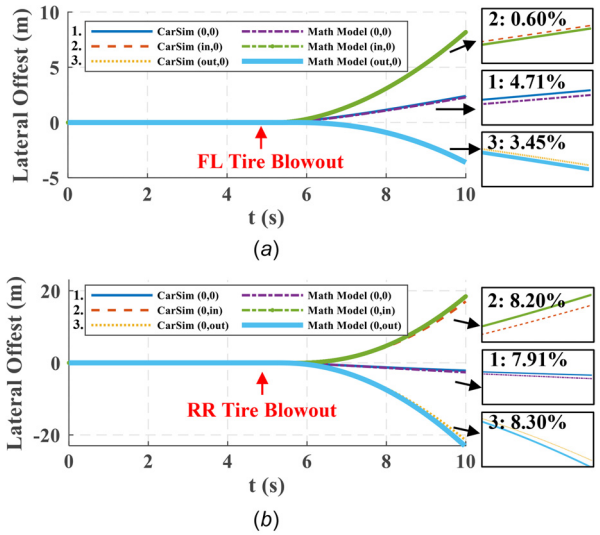

CarSim: different toe angle setups + other fixed alignment parameters
Math Model: different toe angle setups

Fig. 6 Comparison of toe angle impacts with other wheel alignment parameters—case 1: different toe angle setups + other fixed wheel alignment parameters

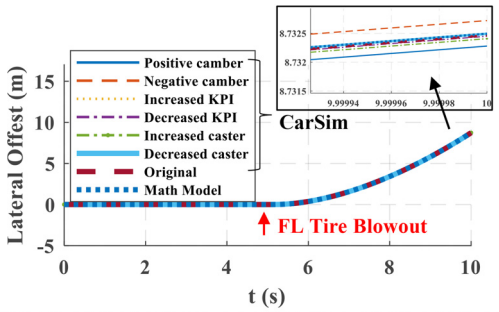

CarSim: fixed toe angle setup + other changed alignment parameters
Math Model: fixed toe angle setup

Fig. 7 Comparison of toe angle impacts with other wheel alignment parameters—case 2: fixed toe angle setup + other changed wheel alignment parameters

setups of camber angle, kingpin inclination angle (KPI), and caster angle in the CARSIM model are 0 deg, 13.5 deg, and 3 deg, respectively. Common variations of these three parameters, namely, 0.5 deg/−0.5 deg camber angles, increased (17 deg) and decreased (10 deg) KPI setups, increased (5 deg) and decreased (1 deg) caster angle setups, were investigated. The driving maneuver and speed are the same as those in the first case, and the front left $(i = 1)$ tire blowout is considered.

In Fig. 7, with a fixed toe angle setup, the results of the CARSIM model with different camber angles, KPI, and caster angles are very close, which indicates that the changes in other wheel alignment parameters have very small impacts on vehicle dynamics (deviation direction and magnitude) after a tire blowout. The lateral offset magnitude is slightly affected and the deviation direction is not impacted at all. Moreover, although the mathematical model does not include the three changed wheel alignment parameters, the result still highly agrees with those of the CARSIM model.

Thus, it is crucial and necessary to explicitly consider the toe angle in the tire blowout model. With fewer impacts, other alignment parameters are negligible. In the following simulation, how different toe angle setups can affect vehicle motions will be explored and analyzed for different tire blowout locations, drivetrains, and driving maneuvers. With the flexibility of selecting different drivetrains in CARSIM, MATLAB/SIMULINK and CARSIM cosimulation are conducted. The adopted CARSIM vehicle, tire blowout duration, and toe angle setups are the same.

3.2 Straight-Line Driving Maneuver. In this section, the vehicle is driven in a straight line at a constant driving speed of 100 km/h (62 mph). The vehicle lateral offsets after the front left $(i = 1)$ tire blowout with different toe angle setups and drivetrains are shown in Fig. 8.

In Fig. 8, for the front left tire blowout, the vehicle does not always deviate to the tire blowout side (left side) with different toe angle setups. Compared with different toe angle setups, only the toe angle setups on the tire-blowout axle (front axle) can significantly affect the lateral offset and deviation direction. For example, the vehicle deviates to the opposite side (right side) with a front toe-out setup. However, the toe angle setups on the non-tire-blowout axle (rear axle) will not have any impact on the lateral offset and deviation direction. Similar results are observed for different drivetrains, such as four wheel drive (4WD), FWD, and RWD.

Since the lateral offset and deviation direction are mainly determined by the lateral forces F_y and the total moment $M_{zx} + M_{zy}$ acting on the vehicle, the force and moment plots for a 4WD vehicle with three different toe setups (e.g., (0, 0), (in, 0), and (out, 0)) are selected to demonstrate the toe angle effects in the tire blowout.

First, the F_y and $M_{zx} + M_{zy}$ for the front left $(i = 1)$ tire blowout with a front zero-toe setup (0, 0) are shown in Figs. 9(*a*) and

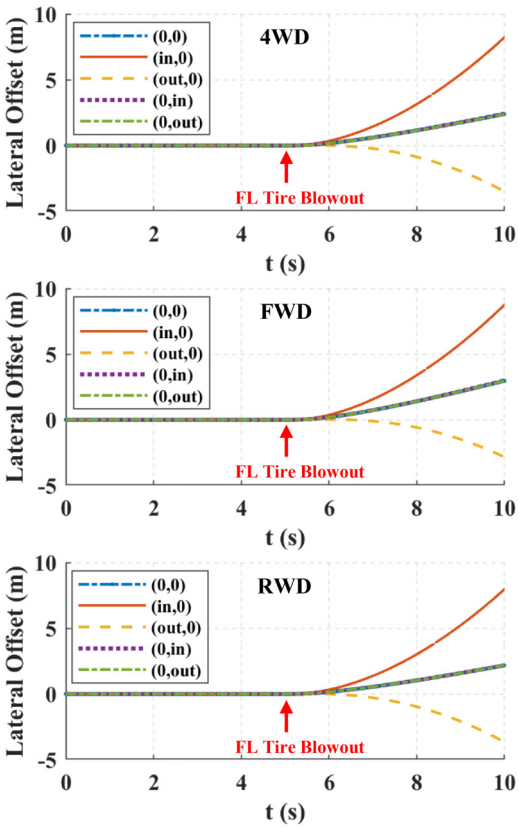

Fig. 8 Lateral offsets of the front left tire blowout with different toe angle setups and drivetrains

9(*b*), respectively. When the tire blowout happens at the fifth second, the rolling resistance force of the blown-out tire increases sharply with the enlarged rolling resistance coefficient. The total moment $M_{zx} + M_{zy}$ mainly consists of the counterclockwise M_{zx}, resulting in a counterclockwise yaw rate r, as shown in Fig. 9(*c*). Given the emerged yaw rate r together with Eq. (6), the positive F_y is generated toward the tire blowout (left) side and the vehicle begins to deviate to the left. Note that the F_{y1} has the smallest magnitude due to the reduction of the lateral stiffness. After F_y is created, the total moment is balanced by the generated M_{zy}. The vehicle keeps deviating to the left driven by the decreasing F_y.

Next, the front left $(i = 1)$ tire blowout with a front toe-in setup (in, 0) is discussed. In Fig. 10(*a*), the toe angle setups can provide symmetric lateral forces for two front tires, with the same magnitude but opposite directions (F_{y1} toward right while F_{y2} toward left). The similar trends as that in Fig. 9(*b*) for the M_{zx}, M_{zy}, and $M_{zx} + M_{zy}$ are observed in Fig. 10(*b*). When the tire blowout happens, the dominated M_{zx} initially introduces a counterclockwise yaw rate r. The F_y of the normal tires $(i = 2, 3, 4)$ are all toward the tire blowout (left) side, while the F_y of the blown-out tire $(i = 1)$ begins to decrease due to the reduction of the tire lateral stiffness. When the M_{zx} and M_{zy} begin to balance, the F_y of four tires begin to reduce. Comparing the front right F_{y2} in Fig. 9(*a*) with that in Fig. 10(*a*), the total lateral force introduced by the front toe-in setup is directed to the left in a larger magnitude (mainly on the front right tire), resulting in an increased lateral offset, as shown in the first plot of Fig. 8.

Last, the front left $(i = 1)$ tire blowout with a front toe-out setup (out, 0) is discussed in Fig. 11. Figure 11(*a*) shows the lateral forces F_y of four tires. When the M_{zx} and M_{zy} starts to balance, the total lateral force introduced by the front toe-out setup is toward the right in a larger magnitude (mainly on the front right tire), resulting in a deviation direction change, as shown in Fig. 8. By comparing Fig. 10(*a*) with Fig. 11(*a*), it is concluded that the lateral offset and deviation direction is mainly determined by the total lateral force, which is dominated by the front right tire with certain initial toe setups. Generally, due to certain toe angle setups, the lateral forces of normal tires on the tire-blowout axle can significantly affect the vehicle lateral offset and deviation direction after a tire blowout.

For the front left tire blowout, the rear toe angle setups do not influence the lateral offset and deviation direction, as shown in Fig. 8. To demonstrate the effect of toe angle setups on the non-tire-blowout axle, the rear toe-in case (0, in) is analyzed. In Fig. 12(*a*), similar analyses can be conducted for the lateral forces on the front tires. However, the lateral forces of the non-tire-blowout rear axle always compensate each other before and after the tire blowout, even with certain toe angle setups. Therefore, the toe angle effect is counteracted for the left and right rear tires, resulting in the same lateral offset and deviation direction as those of the front zero-toe case.

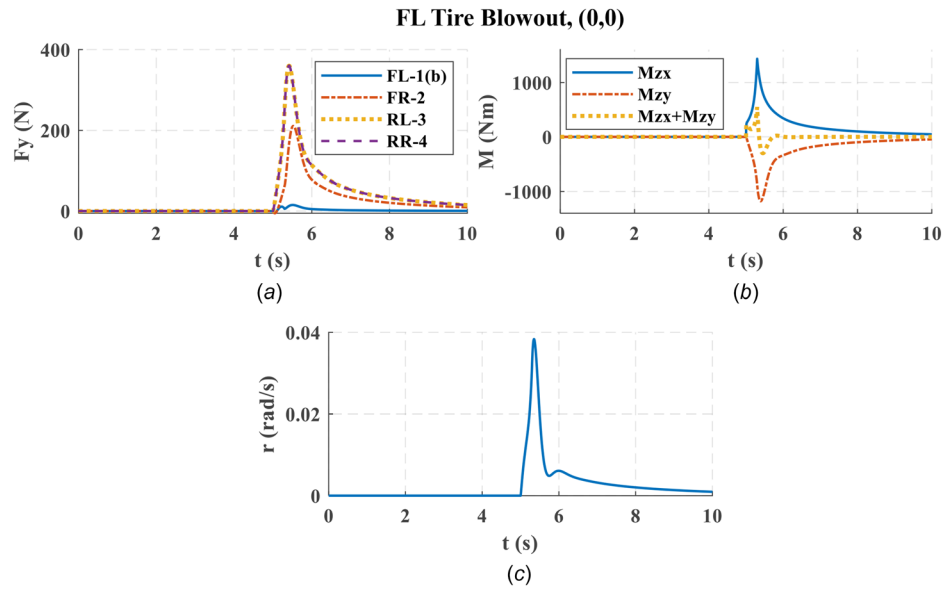

Fig. 9 Lateral forces, moments, and yaw rate of the front left tire blowout with the front zero-toe setup (0, 0)

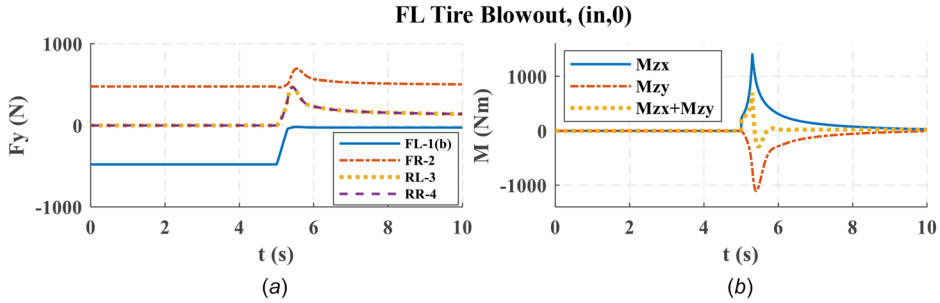

Fig. 10 Lateral forces and moments of the front left tire blowout with the front toe-in setup (in, 0)

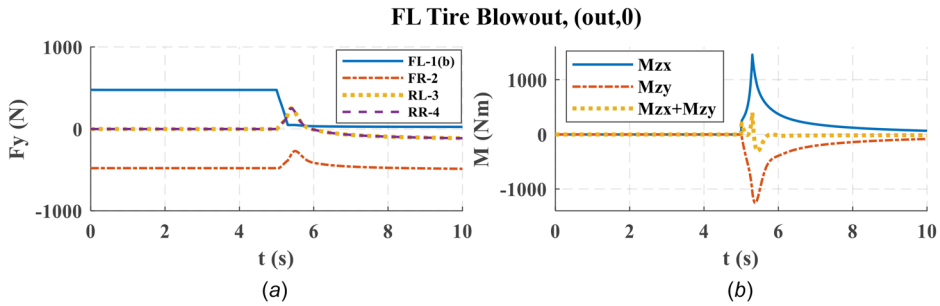

Fig. 11 Lateral forces and moments of the front left tire blowout with the front toe-out setup (out, 0)

In addition to the front left $(i = 1)$ tire blowout case, the rear right tire blowout $(i = 4)$ is also simulated with different toe angle setups and drivetrains. Figure 13 shows the simulation results of lateral offsets. Compared with the studies without toe angle setups, the vehicle would deviate to the tire blowout side. However, the vehicle does not always deviate to the tire blowout side (right) when a certain toe angle setup is applied. The same conclusion, which the toe angle setup on the tire-blowout axle (rear axle in this case) can affect the deviation direction and offset, can still be obtained. For example, the rear toe-in setup can cause the deviation direction change and the rear toe-out can increase the lateral offset for the rear right tire blowout case. The toe angle setups on the other (front) axle and different drivetrains will not influence the lateral offset and deviation direction. Similar force and moment responses could be analyzed, which are not repeated here for simplicity.

3.3 Cornering Maneuver. In this section, the vehicle is driven to make a cornering with a constant 3-deg ground steering angle (to the left) at a low constant driving speed of 40 km/h (25 mph). Front left $(i = 1)$ and rear right $(i = 4)$ tire blowout with different toe angle setups and drivetrains are investigated.

The global coordinates of a 4WD vehicle with different toe angle setups are shown in Fig. 14. The baseline denotes the vehicle trajectory without the tire blowout. Note that the baselines for different toe angle setups are different due to the combination of steering angle and toe angle as described in (5). It is observed that different toe angle setups do not affect the understeering and oversteering trends for the front left $(i = 1)$ tire blowout and rear right $(i = 4)$ tire blowout, respectively. Simulations about FWD and RWD vehicles with different toe angle setups are also analyzed. The same conclusion as that of the 4WD vehicle can be obtained from the simulation results, which are not repeated.

For the front left tire blowout, the front left blown-out tire (a steering tire) cannot provide a sufficient lateral force to maintain the original cornering maneuver. As shown in Fig. 15, the F_{y1} of the blown-out tire reduces largely due to the reduction of the lateral stiffness and vertical force. The F_{y2} of the normal tire on the tire-blowout axle increases with the increase of the vertical force. The F_y of rear two tires have small changes after a tire blowout. Due to the large reduction in F_{y1} (dominated) and the increase in F_{y2}, the total lateral force $F_{y-\text{total}}$ acted on the vehicle becomes less after the tire blowout, leading to the understeering phenomenon.

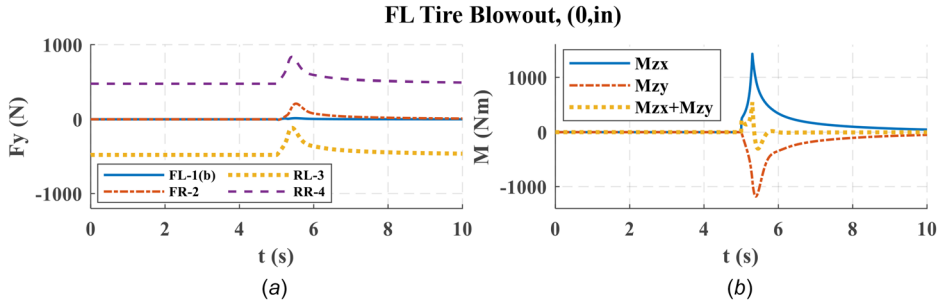

Fig. 12 Lateral forces and moments of the front left tire blowout with the rear toe-in setup (0, in)

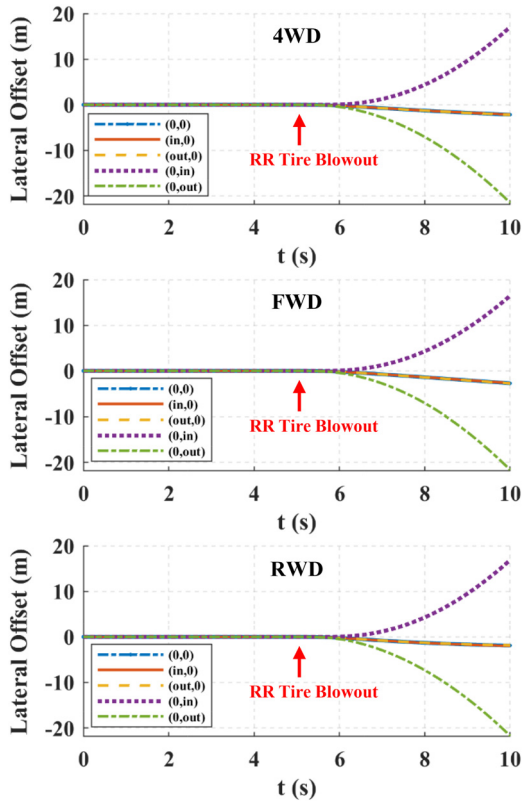

Fig. 13 Lateral offsets of the rear right tire blowout with different toe angle setups and drivetrains

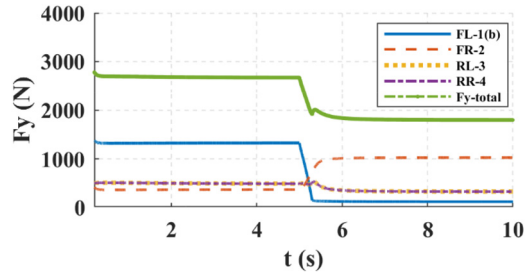

Fig. 15 Lateral forces of the front left tire blowout with the front toe-out setup (out, 0) during cornering maneuver

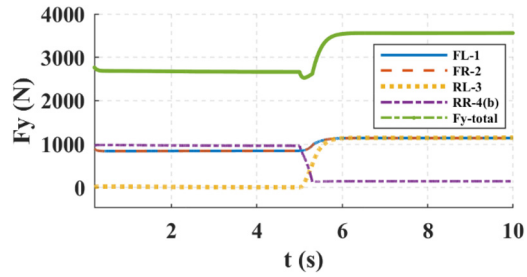

Fig. 16 Lateral forces of the rear right tire blowout with the rear toe-in setup (0, in) during cornering maneuver

For the rear right tire blowout, the front normal tires can provide sufficient lateral forces for cornering. As shown in Fig. 16, the F_y of the front tires have relatively small variations compared with those of the rear tires. The F_{y4} of the blown-out tire decrease sharply with a decrease in its lateral stiffness and vertical force. The F_{y3} of the normal tire on the tire-blowout axle increases with the increase of its vertical force. For the non-steering rear tires,

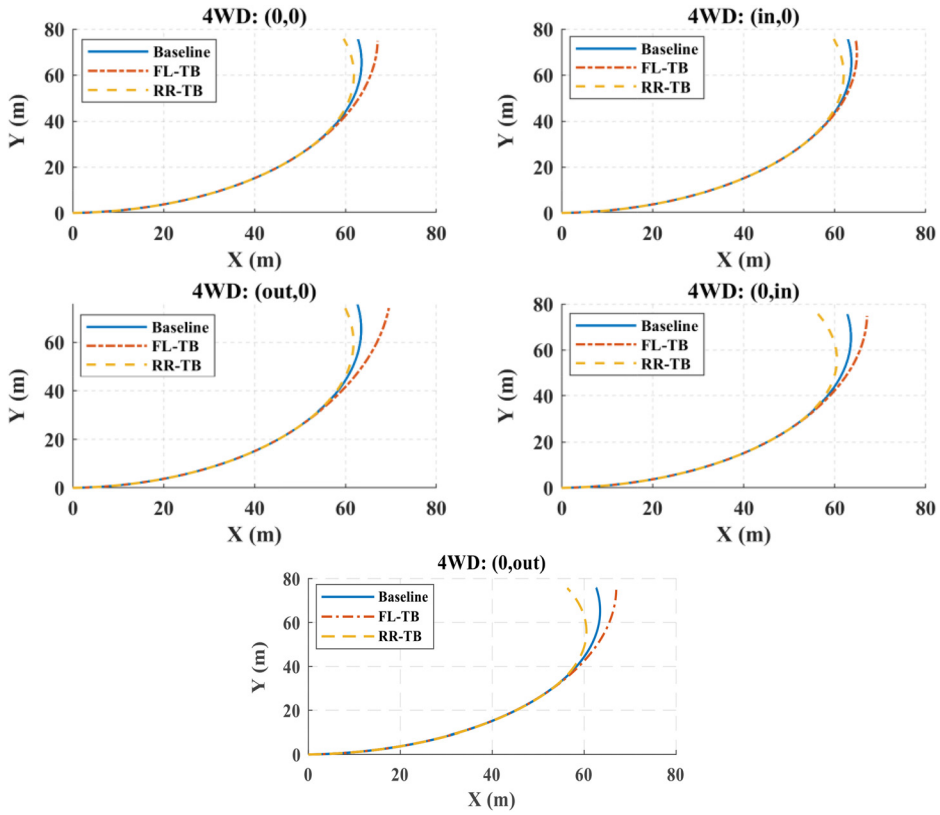

Fig. 14 The trajectories of a 4WD vehicle with different toe angle setups

the increase in F_{y3} is larger than the decrease in F_{y4} and the total lateral force $F_{y-\text{total}}$ on the vehicle increases after a tire blowout, resulting in the oversteering phenomenon.

Since the small toe angle (0.5 deg) is dominated by the large steering angle (3 deg) in cornering maneuvers, the toe angle setups do not influence the vehicle deviation directions after tire blowout.

To the authors' best knowledge, the toe angle effect on the tire blowout is studied for the first time in this work. The general conclusions from the above simulation results are summarized as follows:

(1) In straight-line driving, the toe angle setups on the tire-blowout axle can affect the vehicle lateral offset and deviation direction. Specifically, the front toe-out will cause the right deviation for the front left tire blowout, while the rear toe-in will result in the left deviation for the rear right tire blowout.
(2) Toe angle setups do not influence the understeering (for the front left tire blowout) and the oversteering (for the rear right tire blowout) trends during cornering maneuvers.
(3) The above two conclusions are valid for vehicles with different drivetrains, such as 4WD, FWD, and RWD.

Remark 2. Theoretically, from the Dugoff's tire model in Eqs. (1) and (2), different road surface conditions (different tire-road friction coefficients μ) and tire types (can give different lateral stiffness C_y) will mainly influence the magnitudes of lateral forces and their variations before and after a tire blowout. However, the force variation trend and direction will not be affected, which should be similar to those shown in Figs. 11–13, 15, and 16. The simulations with different road surface conditions (different μ) and different tire types (different C_y) are also conducted. The same conclusions can be drawn from the simulation results, which will not be repeated. Therefore, the aforementioned results and conclusions are still valid for different road surface conditions and tire types.

4 Experimental Results and Discussions

Tire blowout modeling and analyses were mainly investigated via simulation results in the literature. Considering the complex dynamic process, experimental validations on modeling (and control design) of tire blowout will introduce more insights and values. In this paper, to validate the proposed tire blowout model and the conclusions from simulation results in a more convincible and practical manner, multiple tire blowout experiments are conducted on a scaled test vehicle.

Table 2 Parameters of the scaled test vehicle

Parameter	Symbol	Value	Final value
Vehicle parameters			
Vehicle total mass	m	63.2 kg	—
Moment inertia around CG	I_z	7.98 kg/m^2	—
Distance from front axle to CG	l_f	0.388 m	—
Distance from front axle to CG	l_r	0.388 m	—
Wheel track	l_t	0.622 m	—
Height of CG	h_g	0.13 m	—
Front suspension stiffness	K_{sf}	2000 N/m	—
Rear suspension stiffness	K_{sr}	2000 N/m	—
Tire parameters			
Tire effective radius	R_e	0.127 m	To 2/3
Longitudinal stiffness	C_x	600 N/slip	To 1/10
Lateral stiffness	C_y	700 N/rad	To 1/10
Wheel moment inertia	I_w	0.012 kg/m^2	—
Rolling resistance coefficient	K_r	0.018	To 30 times

4.1 Experimental Platform. The experimental platform is shown in Fig. 17. All the hardware is built on a four-wheel-independently actuated scaled test vehicle, which has four driving motors for the wheels. In the experiment, two front driving motors, two rear driving motors, or all four driving motors can be utilized for FWD, RWD, or 4WD drivetrain. Two steering motors are also installed on the front and rear axles, where the rear steering is locked in experiments. The parameters of the scaled test vehicle are shown in Table 2. The test vehicle has relatively large dimensions (1/4–1/3 dimensions of a real vehicle) with air-filled tires and can reach a maximum speed of around 50 km/h. In the development of the test vehicle, weights were successively added (20 pounds each and 3–4 weights were combined differently) on the test vehicle to investigate if the results of different tire blowout

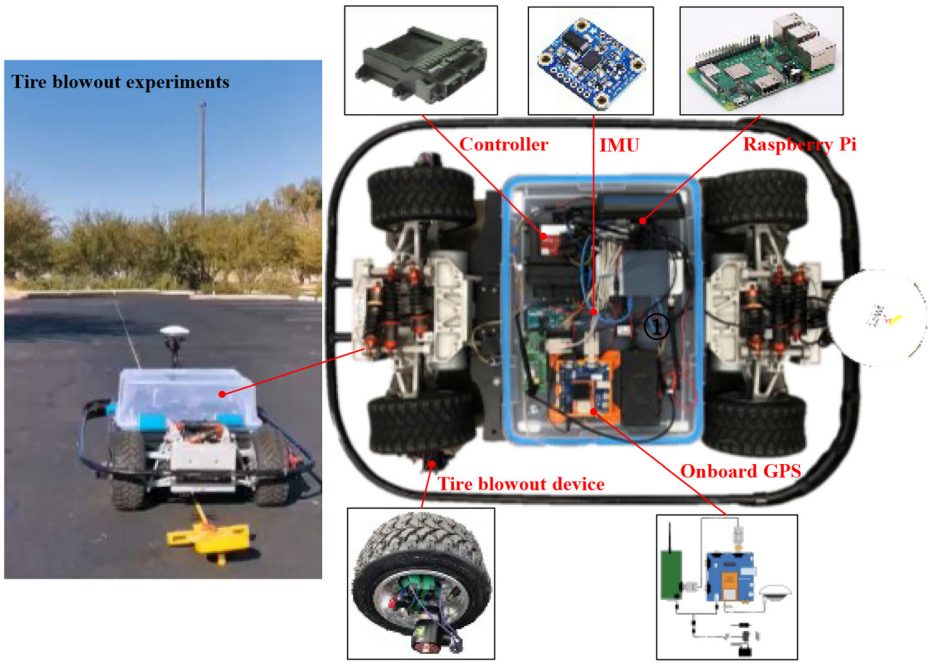

Fig. 17 The experimental platform and tire blowout experiments in the field

experiments would change with different CG and weight distributions. The experimental results about the deviation direction were consistent with those obtained from simulation results by using a real full-size vehicle in CARSIM. Therefore, the experimental platform can effectively represent real vehicle dynamics. In this work, the dynamical similarity of the scaled test vehicle to a full-size C-class vehicle in CARSIM is also mathematically proved through the Buckingham π theory, which is described as follows.

The Buckingham π theory is a convenient tool to justify if two systems of different size scales are dynamically similar without explicitly knowing the accurate dynamic equations of both systems [27–29]. If the dimensionless π groups of variables and parameters are maintained, both systems have a dynamic similarity [27]. With the full-size and scaled vehicle parameters in Tables 1 and 2, some calculations using the π theory are as follows.

The (fixed) wheel tracks of the scaled test vehicle and the full-size vehicle are utilized for non-dimensionalization. The subscripts s and f denote the scaled vehicle and full-size vehicle, respectively. Other parameters can be referred to Tables 1 and 2. Assuming that the vehicle densities are the same, e.g., $\rho_s = \rho_f$, the dimensionless mass $\pi 1$ group is described in the following equation:

$$\left(\frac{\rho_s {l_{ts}}^3}{m_s}\right)_{\text{scaled}} = \left(\frac{\rho_f {l_{tf}}^3}{m_f}\right)_{\text{full-size}}, \; m_s = 72.3\,\text{kg} \tag{15}$$

Similarly, the dimensionless tire effective radius $\pi 2$ and yaw moment of inertial $\pi 3$ groups are calculated in Eqs. (16) and (17), respectively,

$$\left(\frac{R_{es}}{l_{ts}}\right)_{\text{scaled}} = \left(\frac{R_{ef}}{l_{tf}}\right)_{\text{full-size}}, \; R_{es} = 0.121\,\text{m} \tag{16}$$

$$\left(\frac{{I_{zs}}^3}{m_s l_{ts}^2}\right)_{\text{scaled}} = \left(\frac{{I_{zf}}^3}{m_f l_{tf}^2}\right)_{\text{full-size}}, \; I_{zs} = 9.48\,\text{kg}\cdot\text{m}^2 \tag{17}$$

Compared with the calculations, the mass of the scaled vehicle is 12% lighter. Tire effective radius is 5% larger and the yaw moment of inertial is 15% smaller. Other vehicle parameters can be calculated similarly, which are not repeated. Given that the parameters of the scaled test vehicle are close to the expected values from the dynamical similarity calculations, the scaled test vehicle in the experiments is dynamically similar to the full-size C-class vehicle and the real vehicle dynamics can be effectively represented.

On the scaled test vehicle, other hardware is equipped for the tire blowout test. The Swift Navigation® Piksi Multi (San Francisco, CA) global positioning system (GPS) is applied to provide precise global positions, including an onboard GPS and a GPS base station. The control algorithms are programmed in the New Eagle® BCM48 controller to select different drivetrains (FWD, RWD, or 4WD) and achieve the speed and steering controls. The Adafruit® nine degrees-of-freedom Inertial measurement unit is also installed. All the data from the aforementioned sensors together with vehicle controller area network bus signals are collected by the Raspberry Pi and stored in a USB drive. A tire blowout device was designed and installed to remotely trigger a tire blowout during experiments, which includes an air release valve, an air hose, and a radio remote controller. The air inside the tire can be released rapidly in 0.3 s, based on an experimental test. Considering that a real tire blowout typically completes less than 1 s [12,18], the device can sufficiently mimic the explosive and rapid process of a real tire blowout.

To guarantee safety during experiments, a manual remote controller for the scaled test vehicle is utilized, which has a control mode switch. In the automatic control mode, the test vehicle is driven by the control algorithm programmed in the BCM48 controller. Therefore, a tire blowout can be triggered in the straight-line driving maneuver with a constant driving speed and triggered for the cornering maneuver with both a constant driving speed and a constant steering angle. When switching to the manual control mode, a human can quickly take over control of the test vehicle using the remote controller.

4.2 Straight-Line Driving Maneuver. In the straight-line driving maneuver, the tire blowout is triggered when the test vehicle is accelerated to a constant driving speed of 5 m/s. The toe angle is set as 0.5 deg by measuring and adjusting the leading and tail edges of the tire with respect to the vehicle longitudinal axis, as shown in Fig. 1. Other wheel alignment parameters are not changed.

In the following experimental results, tire blowout trigger time and location for each experiment will be labeled in vehicle states plots (time in second in the x-axis) and trajectory plots (X distance in meter in the x-axis), respectively. The baselines in the trajectory plots represent the non-tire-blowout vehicle trajectories with different toe angle setups. Note that the baseline trajectory plots for the straight-line driving maneuver are relatively straight considering the small (Y) deviation along with the long (X) traveling distance. The comparison between the baseline and tire blowout trajectory is the main focus.

The front left tire blowout in 4WD with a front toe-out setup is explored first. The experimental results are shown in Figs. 18 and 19. When the vehicle is accelerated to a constant driving speed of 5 m/s around 7 s in Fig. 18 and travels 10 m in Fig. 19, the tire blowout is triggered. Then, the negative lateral acceleration a_y and lateral speed v_y (toward the right), and the clockwise yaw rate r indicate the vehicle deviates to the right side with a front toe-out setup, as shown in Fig. 19. Driving torques are applied to four wheels. With the decreased tire effective radius of the blown-out front left tire, the wheel rotational speed increases. Note that the x-axis (time) of the vehicle states and control signals are limited to a certain range since the test vehicle is controlled manually for safety purposes after 10 s.

The vehicle trajectories of the front left tire blowout with a front toe-in setup are shown in Fig. 20. For the test vehicle in FWD and RWD with a front toe-out setup, the front left tire blowout experimental results are shown in Figs. 21 and 22, respectively. Considering the trajectories in Figs. 20–22 are consistent with the results of those in the simulation, the vehicle states and control signals are ignored.

From the four different experimental cases, a front toe-out setup is verified to deviate the vehicle to the (opposite) right direction for the front left tire blowout, which is valid for different drivetrains.

Next, the rear right tire blowout in 4WD with a rear toe-in setup is investigated. The test conditions are the same as those for the front left tire blowout. The experimental results are shown in Figs. 23 and 24. When the tire blowout happens around 22 s in Fig. 23 and at 10 m in Fig. 24, the positive lateral acceleration a_y and lateral speed v_y (toward the left), and the counterclockwise yaw rate r indicate the vehicle deviates to the right side with a rear toe-in setup, as shown in Fig. 24. Due to the reduction of the tire effective radius of the blown-out rear right tire, the wheel rotational speed increases. The x-axis (time) in Fig. 23 are also limited since manual control is activated for safety purpose after 25 s.

Moreover, the rear right tire blowout in 4WD with a rear toe-out setup, FWD with a rear toe-in setup, RWD with a rear toe-in setup are also explored. The experimental trajectories are shown in Figs. 25–27, respectively.

From the four different experimental cases, a rear toe-in setup is verified to deviate the vehicle to the (opposite) left direction for the rear right tire blowout, which is valid for different drivetrains.

4.3 Cornering Maneuver. In this section, the tire blowout experiments for cornering maneuvers are conducted. The test

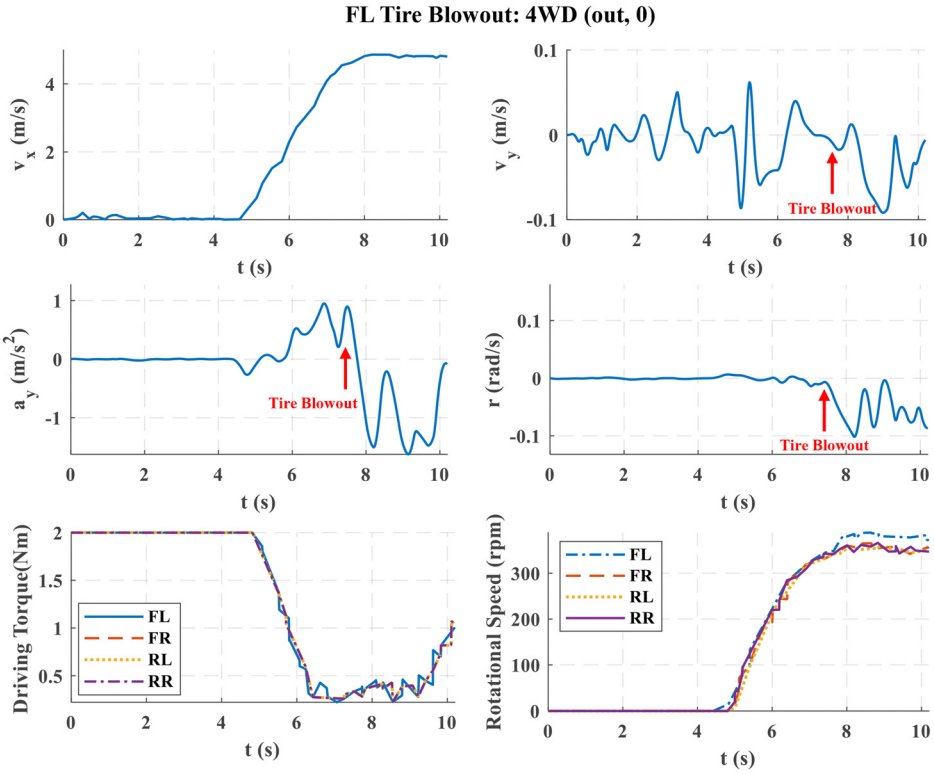

Fig. 18 Vehicle states and control signals of the 4WD vehicle with a front toe-out setup (out, 0) for the front left tire blowout

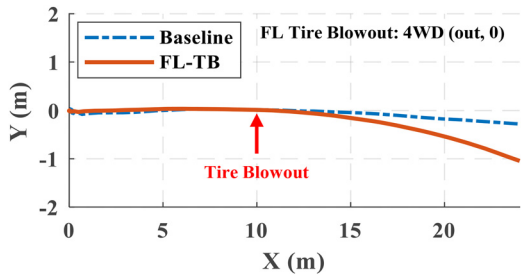

Fig. 19 Trajectories of the 4WD vehicle with a front toe-out (out, 0) setup for the front left tire blowout

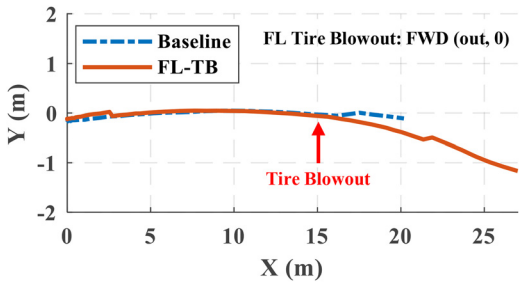

Fig. 21 Trajectories of the FWD vehicle with a front toe-out setup (out, 0) for the front left tire blowout

vehicle is accelerated to a constant driving speed of 3 m/s, then a left steering angle of 11 deg on the ground is applied. Considering that the vehicle speed in experiments (3 m/s) is much less than that (40 km/h, 11 m/s) in simulation for safety reasons, the steering angle is increased to emphasize the cornering behaviors. The toe angle is still set at 0.5 deg. The tire blowout is triggered at a fixed point during the cornering.

The front left tire blowout in 4WD with a front toe-in setup is explored first. The experimental results are shown in Fig. 28. The reduced lateral acceleration a_y and yaw rate r indicate that the front left tire blowout causes an understeering phenomenon.

The trajectory of a front toe-out setup is presented in Fig. 29. The front left tire blowout with front toe-in and front toe-out setups in FWD and RWD were also tested in experiments. Since

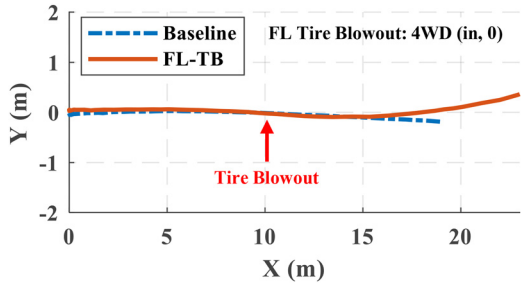

Fig. 20 Trajectories of the 4WD vehicle with a front toe-in setup (in, 0) for the front left tire blowout

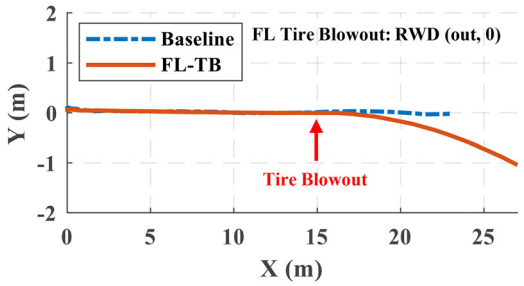

Fig. 22 Trajectories of the RWD vehicle with a front toe-out setup (out, 0) for the front left tire blowout

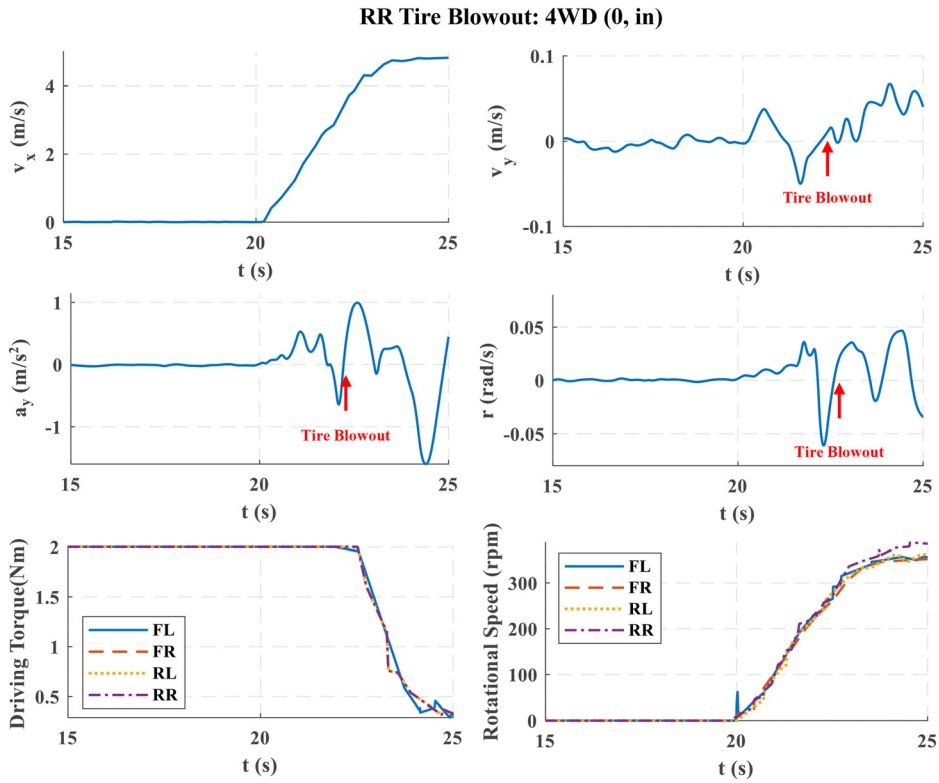

Fig. 23 Vehicle states and signals of the 4WD vehicle with rear toe-in (0, in) setup for rear right tire blowout

similar vehicle states and trajectories were observed, the experimental results are not repeated in this paper.

Next, the rear right tire blowout in 4WD with a rear toe-in setup is explored. The experimental results are shown in Fig. 30. The increased lateral acceleration a_y indicates that the overall lateral force applied on the vehicle after the tire blowout increases, which causes an oversteering phenomenon. The trajectory for a rear toe-out setup is presented in Fig. 31 and an oversteering phenomenon

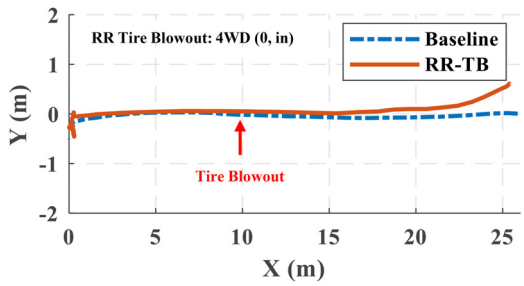

Fig. 24 Trajectories of the 4WD vehicle with a rear toe-in setup (0, in) for the rear right tire blowout

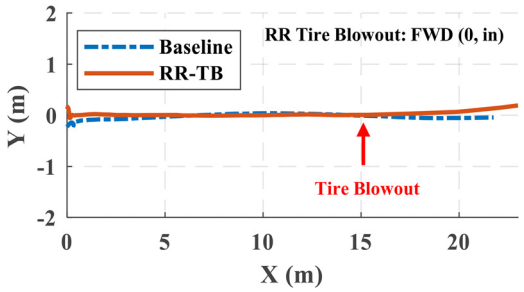

Fig. 26 Trajectories of the FWD vehicle with a rear toe-in (0, in) setup for the rear right tire blowout

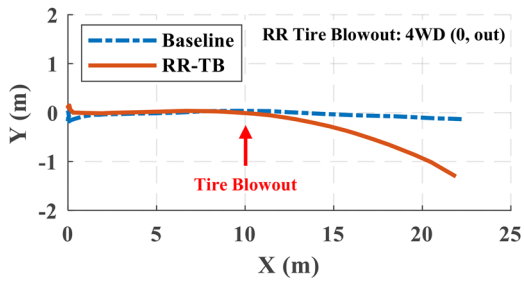

Fig. 25 Trajectories of the 4WD vehicle with a rear toe-out (0, out) setup for the rear right tire blowout

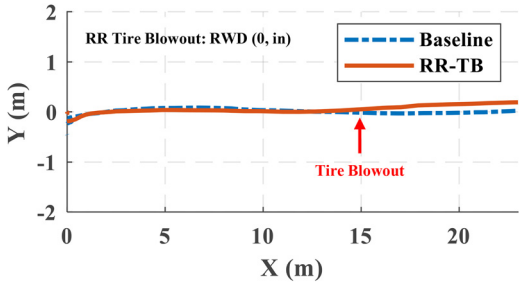

Fig. 27 Trajectories of the RWD vehicle with a rear toe-out (0, in) setup for the rear right tire blowout

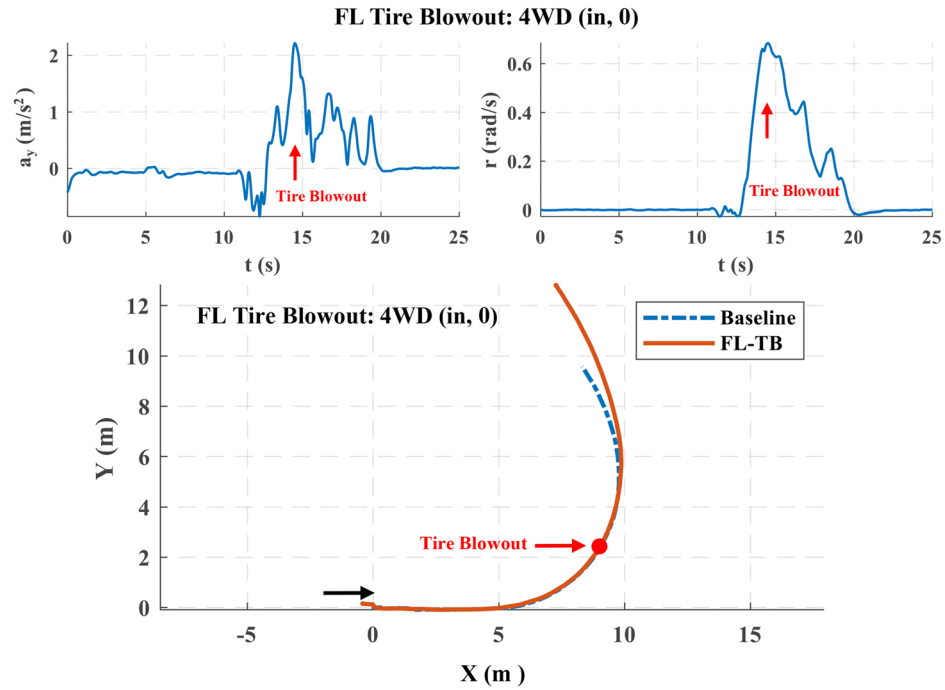

Fig. 28 Experimental results of the 4WD vehicle with a front toe-in (in, 0) setup for the front left tire blowout

is still observed. Due to the similar vehicle states and trajectories, other experimental results for different toe-angle setups and drivetrains are not presented for simplicity.

From the tire blowout experimental results for the cornering maneuver, it is validated that different toe angle setups will not affect the understeering (for the front tire blowout) or the oversteering (for the rear tire blowout) results.

Based on the simulation results of a full-size vehicle and experimental results of the scaled test vehicle, the conclusions are validated by evaluating and comparing the deviation directions. Moreover, the effectiveness of the proposed tire blowout model in describing tire blowout impacts on vehicle dynamics with different toe angle setups is also verified. Although only a scaled vehicle was implemented for experimental validations considering safety, the dynamical similarity of the scaled test vehicle to the full-size vehicle indicates that a full-size vehicle in reality can achieve the same deviation trends with certain toe angle setups as those observed in simulation using a CARSIM vehicle, which was based on a full-size vehicle.

4.4 Evaluations on Model Accuracy. In this section, the accuracy of the proposed tire blowout model with toe angles is experimentally validated. By applying the parameters of the scaled test vehicle (in Table 2) to the proposed tire blowout model together with the vehicle mathematical model (13), simulation results under the same experimental conditions (i.e., same drivetrain, tire blowout scenario, and speed profile) can be obtained. The simulation results will be compared with the experimental results to evaluate the model accuracy in describing tire blowout impacts on vehicle dynamics. Two experiments from Sec. 4.2 are selected for comparison.

In Fig. 32, the baseline of the proposed model is the straight black dash line. In Fig. 32(*a*), for front left tire blowout with front toe-out setup, the final lateral offset compared with the baseline in

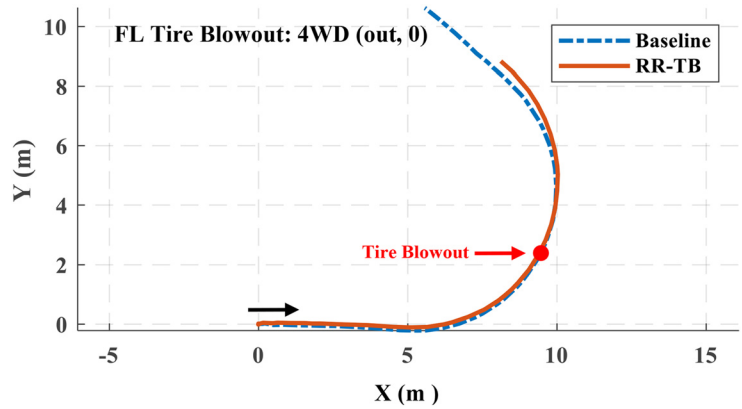

Fig. 29 Experimental results of the 4WD vehicle with a front toe-out (out, 0) setup for the front left tire blowout

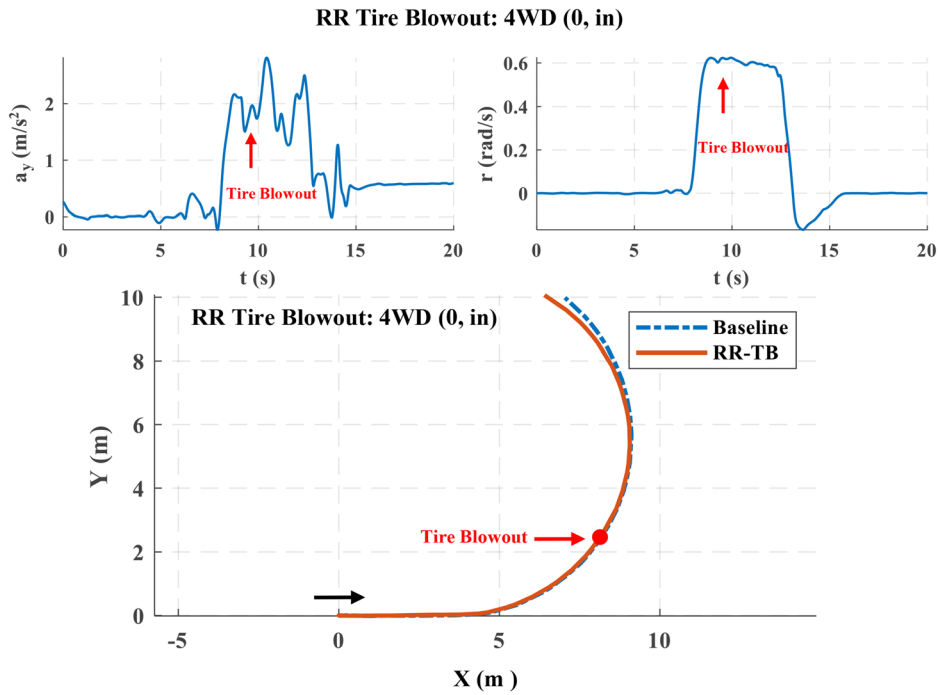

Fig. 30 Experimental results of the 4WD vehicle with a rear toe-in (0, in) setup for the rear right tire blowout

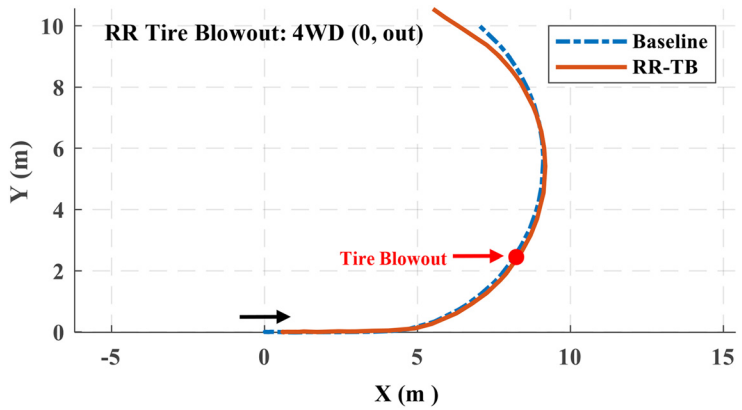

Fig. 31 Experimental results of the 4WD vehicle with a rear toe-out (0, out) setup for the rear right tire blowout

the experiment is 0.72 m and the predicted deviation from the proposed tire blowout model is 0.64 m. The difference is small (0.08 m, 11%) along with the 23 m traveling distance. In Fig. 32(*b*), for rear right tire blowout with rear toe-in setup, the final lateral offset of the test vehicle compared with the baseline is 0.61 m in the experiment, while the predicted deviation using the proposed model is 0.51 m. The difference is still small (0.1 m, 16%) along with the 26 m traveling distance. The good agreements indicate that the proposed tire blowout model can effectively reflect the tire blowout impacts on vehicle dynamics.

5 Conclusions

In this work, the widely applied toe angle setup was explicitly considered and integrated into a tire blowout model. Using the proposed tire blowout model, the simulation results of different case studies indicate that the vehicle will not always deviate to the tire blowout side with certain toe angle setups in a straight-line driving maneuver, since a toe angle setup could provide certain initial lateral forces to the normal tire. With the steering angle dominated in the cornering maneuver, toe angle setups cannot affect understeering (for the front tire blowout) and the oversteering (for the rear tire blowout) phenomena. New findings from simulation results and the accuracy of the proposed tire blowout model were further validated through different tire blowout experiments using a scaled test vehicle. The proposed tire blowout model can serve as a high-fidelity physical model to study different tire blowout impacts and evaluate control performance. Vehicle safety control design for tire blowout will be studied in the future work.

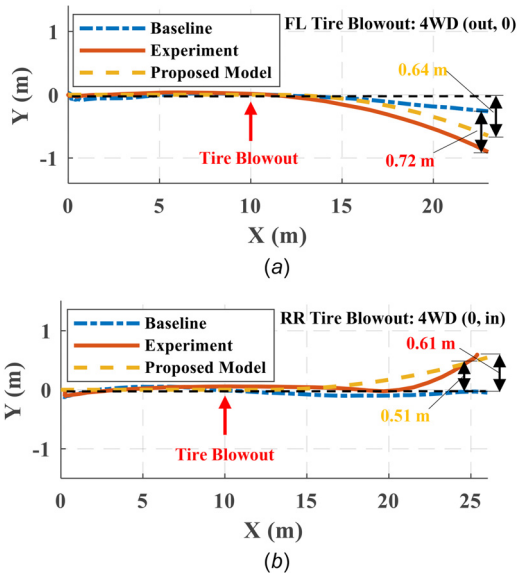

Fig. 32 Accuracy evaluations of the proposed tire blowout model using experimental results

Funding Data

- General Motors Global R&D. National Science Foundation (Grant No. CMMI-2043286; Funder ID: 10.13039/100000001).

Nomenclature

a_x = vehicle longitudinal acceleration (m/s^2)
a_y = vehicle lateral acceleration (m/s^2)
C_x = tire longitudinal stiffness (N/slip)
C_y = tire lateral stiffness (N/rad)
F_{ri} = rolling resistance force of the ith tire (N)
F_{xi} = longitudinal friction force of the ith tire (N)
F_{yi} = lateral friction force of the ith tire (N)
F_{zi} = vertical force of the ith tire (N)
h_g = height of the vehicle center of gravity (m)
h_{si} = suspension height at the ith tire (m)
h_{s0i} = initial suspension height at the ith tire (m)
i = subscripts ($i = 1, 2, 3, 4$) for the front left, front right, rear left, and rear right tires, respectively
I_z = vehicle moment inertia through center of gravity (kg/m^2)
$I_{\omega i}$ = moment of inertia of the ith tire (kg/m^2)
K_r = rolling resistance coefficient
$K_{sk}(k = f, r)$ = front/rear suspension vertical stiffness (N/m)
l_f = distance from the front axle to the vehicle center of gravity (m)
l_r = distance from the rear axle to the vehicle center of gravity (m)
l_t = vehicle wheel track (m)
m = vehicle mass (kg)
M_{zx} = moment portion from tire forces in the x-direction (N·m)
$M_{zx} + M_{zy}$ = total yaw moment applied on the vehicle (N·m)
M_{zy} = moment portion from tire forces in the y-direction (N·m)
r = vehicle yaw rate (rad/s)
R_{ei} = tire effective radius of the ith tire (m)
s_i = slip ratio of the ith tire (%)
v_x = vehicle longitudinal velocity (m/s)
T_i = actuation torque of the ith tire (Nm)
α_i = slip angle of the ith tire (rad)
δ_i = actual steering angle of ith tire (rad)
δ_f = front steering angle (rad)
$\delta_{\text{toe}j}, j = f, r$ = front/rear toe angle (rad)
Δf = load transfer due to tire blowout (N)
Δt = tire blowout duration (s)
v_y = vehicle lateral velocity (m/s)
ω_i = wheel rotational speed of the ith tire (rad/s)

References

[1] Choi, E-H., 2002, "Tire-Related Factors in the Pre-Crash Phase," National Highway Traffic Safety Administration, Washington, DC, Report No. DOT HS 811 617.
[2] Huang, Y., Wang, F., Li, A., Shi, Y., and Chen, Y., 2021, "Development and Performance Enhancement of an Over- Actuated Autonomous Ground Vehicle," IEEE/ASME Trans. Mechatronics, **26**(1), pp. 33–44.
[3] Li, A., Chen, Y., Lin, W.-C., and Du, X., 2020, "Shared Steering Control of Tire Blowout for Ground Vehicles," Proceedings of American Control Conference, Denver, CO, July 1–3, pp. 4862–4867.
[4] Yang, L., Yue, M., Wang, J., and Hou, W., 2019, "RMPC-Based Directional Stability Control for Electric Vehicles Subject to Tire Blowout on Curved Expressway," ASME J. Dyn. Syst., Meas., Control, **141**(4), p. 041009.
[5] Tagesson, K., Jacobson, B., and Laine, L., 2014, "Driver Response at Tyre Blow-Out in Heavy Vehicles & the Importance of Scrub Radius," Proceedings of IEEE Intelligent Vehicles Symposium, Dearborn, MI, June 8–11, pp. 1157–1162.
[6] Wang, F., Chen, H., and Cao, D., 2016, "Nonlinear Coordinated Motion Control of Road Vehicles After a Tire Blowout," IEEE Trans. Control Syst. Technol., **24**(3), pp. 956–970.
[7] Orengo, F., Ray, M. H., and Plaxico, C. A., 2003, "Modeling Tire Blow-Out in Roadside Hardware Simulations Using LS-DYNA," ASME Paper No. IMECE2003-55057.
[8] Wang, F., and Chen, Y., 2019, "Vehicle Rollover Propensity Detection Based on a Mass-Center-Position Metric: A Continuous and Completed Method," IEEE Trans. Veh. Technol., **68**(9), pp. 8652–8662.
[9] Davis, S., 2014, "How Many People Die Each Year Because of Tire Blowout?," accessed Aug. 29, 2014, https://www.standavislaw.com/how-many-people-die-each-year-because-of-tire-blowouts
[10] Patwardhan, S., Tomizuka, M., Zhang, W. B., and Devlin, P., 1994, "Theory and Experiments of Tire Blow-Out Effects and Hazard Reduction Control for Automated Vehicle Lateral Control System," Proceedings of American Control Conference, Baltimore, MD, June 29–July 1, pp. 1207–1209.
[11] Patwardhan, S., Tan, H. S., and Tomizuka, M., 1997, "Experimental Results of a Tire-Burst Controller for AHS," Control Eng. Pract., **5**(11), pp. 1615–1622.
[12] Li, A., Chen, Y., Du, X., and Lin, W.-C., 2021, "Enhanced Tire Blowout Modeling Using Vertical Load Redistribution and Self-alignment Torque," ASME Lett. Dyn. Syst. Control, **1**(1), p. 011001.
[13] Blythe, W., Day, T. D., and Grimes, W. D., 1998, "3-Dimensional Simulation of Vehicle Response to Tire Blow-Outs," SAE Paper No. 980221.
[14] Lozia, Z., 2005, "Simulation Tests of Biaxial Vehicle Motion after a 'Tire Blow-Out'," SAE Paper No. 2005-01-0410.
[15] Wang, F., Chen, H., Guo, H., and Cao, D., 2015, "Constrained H∞ Control for Road Vehicles After a Tire Blow-Out," Mechatronics, **30**, pp. 371–382.
[16] Mo, T., Zhang, X., Fan, K., Mo, W., and Qiu, Y., 2013, "Design and Simulation of the Sliding Mode Controller for the Vehicle Blow-Out Process Control," Int. J. Veh. Saf., **6**(4), pp. 333–346.
[17] Chakravarthy, K. V., 2013, "Development of a Steer Axle Tire Blowout Model for Tractor Semitrailers in TruckSim," Ph.D. dissertation, The Ohio State University, Columbus, OH.
[18] Cai, Y., Zang, M., and Duan, F., 2015, "Modeling and Simulation of Vehicle Responses to Tire Blowout," Tire Sci. Technol., **43**(3), pp. 242–258.
[19] Genta, G., and Morello, L., 2009, The Automotive Chassis, Springer, Berlin, Germany.
[20] Stone, R., and Ball, J. K., 2004, *Automotive Engineering Fundamentals*, SAE International, Warrendale, PA.
[21] Frazee, I., Landon, W., and Hafferkamp, G., 1951, *Automotive Suspensions, Steering, and Wheel Alignment*, American Technical Society, Chicago, IL.
[22] Liu, W., 2001, *The Design of Automotive*, Tsinghua University Press, Beijing, China.
[23] Rajamani, R., 2012, *Vehicle Dynamics and Control*, Springer Science/Business Media, New York.
[24] Yuen, T. J., Foong, S. M., and Ramli, R., 2014, "Optimized Suspension Kinematic Profiles for Handling Performance Using 10-Degree-of-Freedom Vehicle Model," Proc. Inst. Mech. Eng., Part K J. Multi-body Dyn., **228**(1), pp. 82–99.
[25] Doumiati, M., Victorino, A., Charara, A., and Lechner, D., 2009, "Lateral Load Transfer and Normal Forces Estimation for Vehicle Safety: Experimental Test," Veh. Syst. Dyn., **47**(12), pp. 1511–1533.
[26] Chen, Q., Li, X., Zhao, G., and Weaver, J. M., 2015, "Model of Resisting Additional Yaw Torque After Tyre Blowout on a Vehicle," Int. J. Vehicle Safety, **8**(1), pp. 55–64.
[27] R Verma, R., Del Vecchio, D., and Fathy, H. K., 2008, "Development of a Scaled Vehicle With Longitudinal Dynamics of an HMMWV for an ITS Testbed," IEEE/ASME Trans. Mechatronics, **13**(1), pp. 46–57.
[28] Phanomchoeng, G., and Rajamani, R., 2014, "Real-time Estimation of Rollover Index for Tripped Rollovers With a Novel Unknown Input Nonlinear Observer," IEEE/ASME Trans. Mechatronics, **19**(2), pp. 743–754.
[29] Zhao, J., Wang, F., Yu, B., Tong, P., and Chen, K., 2015, "Experimental Study on the Ride Comfort of a Crawler Power Chassis Scale Model Based on the Similitude Theory," Chin. J. Mech. Eng., **28**(3), pp. 496–503.